

# Numerical Investigation of Enhanced Efficiency in CIGS Solar Cells with 3C-SiC and PEDOT:PSS Integration

Rafik Zouache<sup>1</sup>, Okba Saidani<sup>1</sup>, Abderrahim Yousfi<sup>1\*</sup>, Abdullah Saad Alsubaie<sup>2</sup>,  
Ben Abdelmoumene Soulef<sup>1</sup>, Lamari Ferial<sup>1</sup>, Rasidul Islam<sup>3</sup>

<sup>1</sup> ETA Laboratory, Department of Electronics, Faculty of Sciences and Technology, University of Mohamed El Bachir El Ibrahimi, 34030 Bordj Bou Arréridj, P.O.B. 014, Algeria

<sup>2</sup> Department of Physics, College of Khurma University College, Taif University, 21944 Taif, P.O.B. 145, Saudi Arabia

<sup>3</sup> Department of Electrical and Electronic Engineering, Bangamata Sheikh Foijlatunnesa Mujib Science & Technology University, 2012 Jamalpur, P.O.B. 328, Bangladesh

\* Corresponding author, e-mail: [abderrahim.yousfi@univ-bba.dz](mailto:abderrahim.yousfi@univ-bba.dz)

Received: 07 November 2024, Accepted: 30 January 2025, Published online: 20 February 2025

## Abstract

Copper indium gallium selenide (CIGS)-based thin-film solar cells continue to lead advancements in the efficiency of thin-film technologies. In this study, we propose cubic silicon carbide (3C-SiC) as a viable alternative to cadmium sulfide (CdS) for use as a buffer layer in CIGS solar cells. 3C-SiC offers superior transparency, higher electron mobility, and non-toxicity, making it a promising candidate for enhancing device efficiency. In this paper, we present a computational analysis of a thin-film solar cell utilizing a ZnO/3C-SiC/CIGS/ poly(3,4-ethylenedioxythiophene) (PEDOT): polystyrene sulfonate (PSS)/Mo heterostructure with PEDOT:PSS as the back surface field (BSF) layer. Simulations conducted using SCAPS-1D software demonstrate impressive photoconversion efficiencies, achieving an ideal efficiency ( $\eta$ ) of 32.83%, an open circuit voltage ( $V_{oc}$ ) of 0.86 V, a short circuit current density ( $J_{sc}$ ) of 56.40 mA cm<sup>-2</sup>, and a fill factor (FF) of 80.79%. The study systematically examines the influence of key parameters, including CIGS absorber thickness, PEDOT:PSS thickness, 3C-SiC thickness, and temperature, demonstrating a strong correlation with previous experimental results. These findings offer valuable insights for enhancing the performance of CIGS solar cells and highlight promising avenues for future advancements in thin-film photovoltaics.

## Keywords

CIGS, 3C-SiC, PEDOT:PSS, SCAPS-1D, efficiency

## 1 Introduction

Thin films, such as copper indium gallium selenide (CIGS) and cadmium telluride (CdTe), are widely used in solar cells due to their cost-effectiveness and stability. CIGS solar cells demonstrate experimental and simulated efficiencies of 19.55% and 29.31%, respectively, surpassing other thin-film technologies. This superiority is attributed to their stability, high conversion efficiency, low production costs, and environmental benefits. In contrast, monocrystalline silicon solar cells dominate the market with efficiencies exceeding 26%, benefiting from well-established manufacturing processes and exceptional stability [1, 2]. Silicon heterojunction cells, which incorporate thin amorphous silicon films on crystalline silicon, demonstrate how thin-film technology can enhance traditional silicon-based devices. While silicon remains the leading material, its higher cost and the requirement for thicker layers position CIGS as an appealing

alternative for scalable, flexible, and lightweight applications [3, 4]. Moreover, they exhibit resilience under lower irradiance, drawing interest from photovoltaic researchers due to their excellent optoelectronic characteristics, such as a high absorption coefficient, tunable bandgap, and minimal material usage [5]. The bandgap of CIGS can be modified by changing the concentrations of indium and gallium, which are directly influenced by the alloy stoichiometry [6]. Conversely, copper vacancies induce a *p*-type nature in the chalcopyrite configuration of CIGS [7]. Distortion in the lattice constant ratio (*c/a*) of the CIGS structure, as well as the bonding among Ga-Se, In-Se, and Cu-Se, contributes to tetragonal distortion [8, 9]. However, variations in CIGS composition can lead to conduction band mismatches with adjacent layers, negatively impacting photovoltaic performance [10]. In solar cells with CIGS, the buffer layer often

comprises cadmium sulfide, which provides benefits that enhance device efficiency and performance [11]. CdS, being an *n*-type semiconductor, facilitates electron transport, thereby improving overall efficiency [12, 13]. The formation of a heterojunction between the *p*-type CIGS absorber material and the transparent conductive oxide (TCO) layer creates an electron flow path, reducing recombination losses and improving the efficiency of charge carrier collection [14]. Additionally, CdS acts as a passivation material in the CIGS absorber layer, reducing surface defects and trap states, thereby decreasing recombination losses at the CIGS/CdS interface and increasing carrier lifetime, which leads to improved device performance [15, 16]. However, while CdS is widely used as a buffer material for *p*-type CIGS absorbers, it presents inherent issues: firstly, it contains the toxic element cadmium, posing risks of environmental contamination during production, use, and disposal if proper protocols are not followed [17]. Secondly, its relatively wide bandgap energy (~2.4 eV) may reduce the absorption of short-wavelength photons that the CIGS could otherwise absorb more effectively. In light of these challenges, researchers are exploring alternative buffer layer materials with characteristics such as a higher bandgap, environmental friendliness, comparable or superior optoelectronic properties to CdS, and suitability for low-cost fabrication methods [18]. For example, kesterite solar cells lack CdS but typically exhibit lower open circuit voltage ( $V_{oc}$ ) and fill factor (FF) compared to CdS-based ones. However, they manage to achieve higher short circuit current density ( $J_{sc}$ ) due to their larger bandgap [19–21]. Although polycrystalline II-VI semiconductor materials have been used as insulating layers to improve solar cells, the emergence of a new layer of cubic silicon carbide (3C-SiC), which acts as a light-guiding layer, has provided significant advantages in enhancing solar cell efficiency [22]. 3C-SiC not only improves light absorption and its conversion into electrical energy but also offers excellent thermal and chemical stability, which boosts the stability of the solar cell's performance under various operating conditions [23]. Thin layers of cubic silicon carbide also provide effective protection against corrosion and oxidation, extending the cell's lifespan and improving long-term efficiency [24].

This work introduces a novel approach to simulating CIGS-based solar cells by incorporating a 3C-SiC buffer layer and employing back surface field (BSF) layer by utilizing poly(3,4-ethylenedioxythiophene) (PEDOT):polystyrene sulfonate (PSS), a conductive polymer with excellent transparency and tunable electrical properties [25, 26].

Utilizing the SCAPS-1D simulator [27], these simulations reveal that heterostructures consisting of ZnO/3C-SiC/CIGS/PEDOT:PSS/Mo demonstrate impressive photo-conversion efficiency. Furthermore, a detailed analysis explores the influence of various factors such as CIGS thickness, PEDOT:PSS thickness, 3C-SiC thickness, and temperature. These studies provide valuable insights into the intricate relationships between these variables, shedding light on their impact on the stability and efficiency of photovoltaic solar cells (PSCs). Ultimately, this comprehensive simulation study enhances our understanding of the complexities associated with these solar cells and presents promising avenues for future research and development in CIGS-based photovoltaics.

## 2 Device settings and simulation process

In the simulation process using SCAPS-1D software [27], the work functions of the front contact (ZnO) and back contact (Mo) materials were explicitly defined to reflect their actual material properties. This approach ensured realistic boundary conditions, rather than assuming a flat band condition. ZnO was selected for its effectiveness in electron extraction, while Mo was chosen for its efficiency in hole collection. Together, these choices contribute to an accurate modelling of charge carrier transport and help reduce potential contact barriers, which are essential for optimal performance. These materials align with the energy levels of the CIGS absorber and the PEDOT BSF layer, thereby minimizing recombination losses at the interfaces. Integrating the appropriate work functions enhances the reliability of the simulated results. The SCAPS-1D software [27] is instrumental in simulating the behavior of a ZnO/3C-SiC/CIGS/PEDOT:PSS/Mo solar cell. This structure comprises a ZnO window layer was treated as a TCO with a wide band gap of 3.30 eV, a thickness of 20 nm, and a donor density of  $1 \times 10^{18}$ , the *n*-type 3C-SiC buffer layer was taken using 50 nm-thick and  $1 \times 10^{20} \text{ cm}^{-3}$  donor density with a gap of 2.3 eV, the CIGS is a *p*-type semiconductor with 1  $\mu\text{m}$ -thick and  $1 \times 10^{14} \text{ cm}^{-3}$  acceptor density, and a moderate band gap  $E_g = 1.2$  eV, a highly doped BSF layer of PEDOT:PSS(*p*<sup>+</sup>) with a thickness of 100 nm, a hole density of  $1 \times 10^{18} \text{ cm}^{-3}$ , and a band gap of 1.6 eV were displayed in Fig. 1, which together form a *p-n* junction essential for charge carrier separation. The molybdenum back contact facilitates efficient charge carrier extraction. Parameters such as thickness and doping concentration were meticulously input into SCAPS-1D [27], simulating conditions at 300 K under AM1.5G illumination to ensure accurate predictions of device behavior [28].

Front contact	n-ZnO	$10^{18} \text{ cm}^{-3}$ (0.02 $\mu\text{m}$ )
Buffer layer	n-3C-SiC	$10^{20} \text{ cm}^{-3}$ (0.05 $\mu\text{m}$ )
Absorber layer	p-CIGS	$10^{14} \text{ cm}^{-3}$ (1 $\mu\text{m}$ )
BSF	p-PEDOT:PSS	$10^{18} \text{ cm}^{-3}$ (0.1 $\mu\text{m}$ )
Back contact	Mo	(0.1 $\mu\text{m}$ )

Fig. 1 CIGS solar cell configuration

The SCAPS-1D software [27] conducts device simulations in distinct sections, comprising various panels that allow users to adjust parameters and assess outcomes. The underlying theory of this program involves solving the Poisson equation (Eq. (1)), as well as the continuity equations for holes (Eq. (2)) and electrons (Eq. (3)) [29, 30]:

$$\frac{d}{dx} \left( \varepsilon(x) \frac{d\psi}{dx} \right) = q \left[ \begin{matrix} p(x) - n(x) + N_d^+(x) \\ -N_a^-(x) + P_t(x) - n_t(x) \end{matrix} \right], \quad (1)$$

$$-\frac{1}{J} \frac{dJ_p}{dx} + R_p(x) - G(x) = 0, \quad (2)$$

$$-\frac{1}{J} \frac{dJ_n}{dx} + R_n(x) - G(x) = 0, \quad (3)$$

where  $\varepsilon$  signifies dielectric permittivity,  $q$  represents the charge of carriers,  $\psi$  indicates the electrostatic potential,  $R_n$  and  $R_p$  stand for electron and hole recombination rates respectively,  $G$  stands for the generation rate,  $n$  and  $p$  for free electrons and holes, and  $n_t$  and  $P_t$  for trapped electrons and holes,  $N_d^+$  and  $N_a^-$  stand for ionized donor and acceptor doping concentrations, and  $J_n$  and  $J_p$  signify electron and hole current densities [31, 32].

### 3 Interpretation of the results

#### 3.1 Energy band diagram

To comprehend the functioning and ensure the reliability of any semiconductor device, it is essential to refer to the band diagram. In the current work, the band diagram of the simulated design was generated using SCAPS-1D software [27], as shown in Fig. 2. The CIGS absorber material and the PEDOT BSF exhibit excellent band alignment. After adding a thin layer of BSF to PEDOT, a gradient was formed that rose to the surface, repelling electrons away from it, as

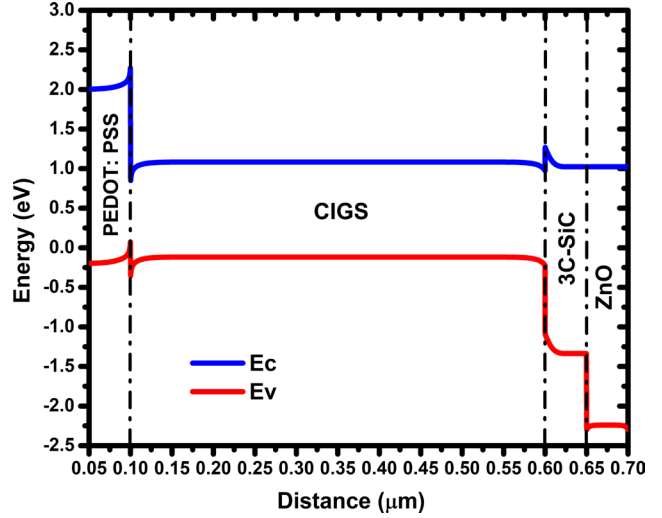


Fig. 2 Band diagram of the proposed design exploiting PEDOT:PSS (BSF)

shown in Fig. 2 [33]. The built-in electric field created on the backside prevents minority carriers from advancing towards the rear surface, which is characterized by a high recombination rate. Consequently, the rear surface reflects electrons away, thereby reducing recombination at this interface [34]. Table 1 presents the electrical properties and geometric parameters of the materials used.

#### 3.2 Influence of CIGS thickness

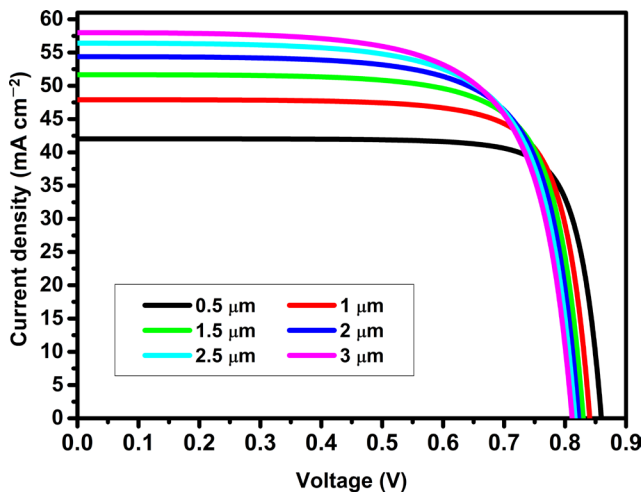
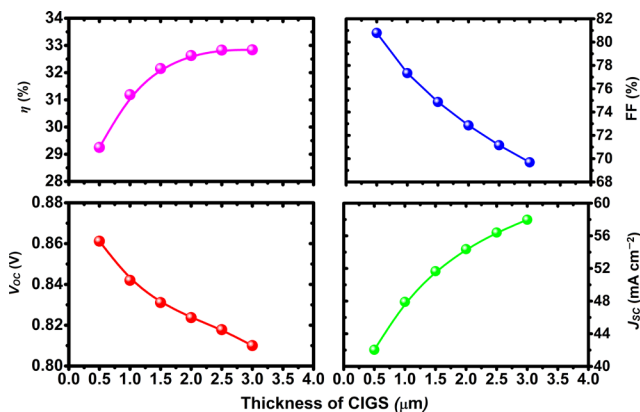
The impact of altering the thickness of the CIGS absorber layer on the  $J$ - $V$  characteristics is shown in Fig. 3. Notably, the curves maintain a consistent shape across various thicknesses of CIGS, while there is a noticeable increase in  $J_{sc}$  as the CIGS thickness increases. This phenomenon occurs because increasing the thickness of the CIGS material effectively enlarges the volume of the absorbing material [35]. Consequently, this expansion facilitates greater photon absorption, leading to a higher current output. However, alongside this increase in current, there is a simultaneous decrease in  $V_{oc}$ . This decline in  $V_{oc}$  is a consequence of the thicker CIGS layer [36]. The maximum efficiency achieved is 32.83% with a CIGS thickness of 3  $\mu\text{m}$ . While a greater thickness can absorb more photons, it also results in a longer distance for charge carriers to travel before reaching the electrodes. This increased distance introduces additional resistance, which subsequently reduces the voltage output.

Fig. 4 illustrates how the thickness of the absorber affects the device's performance. It is evident that the maximum efficiency achieved is 32.83% when the CIGS layer has a thickness of 3  $\mu\text{m}$ . However, efficiency notably

**Table 1** Simulation parameters utilized in the present study at a temperature of 300 K\*

Parameters	ZnO ( <i>n</i> )	3C-SiC ( <i>n</i> )	CIGS ( <i>p</i> )	PEDOT:PSS ( <i>p</i> <sup>+</sup> )
Thickness (μm)	0.02	0.05*	1*	0.1*
Electron affinity (eV)	4.6	4.2	4.5	3.4
Band gap energy (eV)	3.3	2.3	1.2	1.6
Relative permittivity ( $\epsilon_r$ )	9	9.72	13.6	3
Density of states at conduction band ( $N_c$ ) (cm <sup>-3</sup> )	$2.2 \times 10^{18}$	$1 \times 10^{19}$	$1.8 \times 10^{18}$	$2.2 \times 10^{18}$
Density of states at valence band ( $N_v$ ) (cm <sup>-3</sup> )	$1.8 \times 10^{19}$	$5 \times 10^{20}$	$2.2 \times 10^{18}$	$1.8 \times 10^{19}$
Electron mobility (cm <sup>2</sup> V <sup>-1</sup> s <sup>-1</sup> )	100	900	100	0.045
Hole mobility (cm <sup>2</sup> V <sup>-1</sup> s <sup>-1</sup> )	50	40	25	0.045
Doping density ( $N_D/N_A$ ) (cm <sup>-3</sup> )	$1 \times 10^{18}$	$1 \times 10^{20}$	$1 \times 10^{14}$	$1 \times 10^{18}$
Defect density (cm <sup>-3</sup> )	$1 \times 10^{14}$	$1 \times 10^{15}$	$1 \times 10^{14}$	$1 \times 10^{14}$

\* A variable field

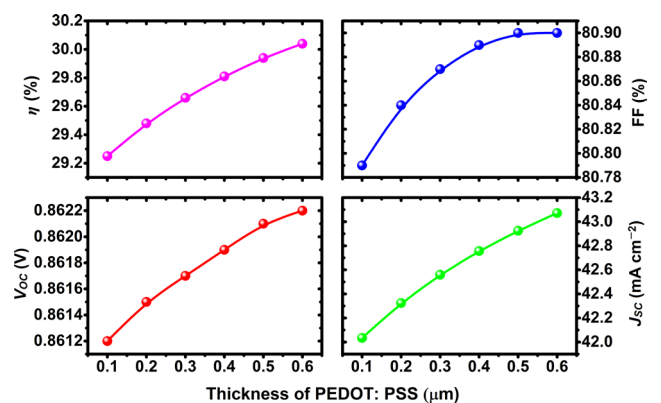

**Fig. 3** The  $J$ - $V$  characteristic influenced by CIGS thickness

**Fig. 4** Influence of CIGS thickness on  $V_{OC}$ ,  $J_{SC}$ , FF, and  $\eta$ 

decreases as the thickness of the CIGS material is reduced. For thicknesses ranging from 0.5 μm to 3 μm, efficiency fluctuates from 29.25% to 32.83%, while the FF decreases from 80.79% to 71.16%. This observation underscores the importance of selecting an optimal absorber thickness to achieve peak electrical efficiency [37]. In this context, it is imperative to choose a thickness exceeding 3 μm. This ensures that the solar cell can effectively capture and

convert incident sunlight into electrical energy, maximizing its overall performance [38].

### 3.3 Effect of PEDOT:PSS layer thickness

Fig. 5 demonstrates the impact of how changing the PEDOT:PSS (BSF) thickness on cell performance. As the thickness of the PEDOT:PSS layer varies within the range of 0.1 to 0.6 μm, several key parameters of cell performance exhibit notable changes. Specifically, there is an observed increase in  $\eta$ ,  $V_{OC}$ , FF, and  $J_{SC}$ . The function of the PEDOT layer as the solar cell's BSF material is responsible for these improvements. Increasing the PEDOT layer's thickness contributes to enhanced charge carrier extraction and collection, which leads to an increased  $J_{SC}$ . This is because the thicker BSF layer helps reduce recombination losses and improves photocurrent generation [1]. Moreover, a thicker PEDOT:PSS layer also enhances the surface passivation of the CIGS solar cell, resulting in reduced surface recombination losses and an increased  $V_{OC}$ . Additionally, the FF, which indicates how well the cell converts light into electricity, also improves with increasing PEDOT:PSS layer thickness. This improvement


**Fig. 5** Effect of PEDOT thickness on  $V_{OC}$ ,  $J_{SC}$ , FF, and  $\eta$

reflects a reduction in resistive losses within the cell [39], leading to an efficiency of up to 30.05% for a 0.6  $\mu\text{m}$ .

### 3.4 Effect of layer thickness of 3C-SiC

Fig. 6 depicts the impact of changing the 3C-SiC thickness on cell performance. As the thickness of the 3C-SiC layer is adjusted within the range of 0.5 to 3  $\mu\text{m}$ , several significant changes in key performance parameters become apparent. Firstly, A slight decrease in efficiency  $\eta$  was observed, from 29.25% to 28.76%. Efficiency represents the solar cell's ability to convert incident light into usable electrical energy [40]. This decrease in efficiency indicates that increasing the 3C-SiC thickness may be contributing to reduced performance. This could be due to increased absorption or reflection of incident light within the thicker buffer layer, resulting in reduced light absorption by the active layers of the solar cell. Additionally, a decrease in  $J_{sc}$  is noted.  $J_{sc}$  represents the maximum current that can be generated by the solar cell when it is short-circuited [41]. The decrease in  $J_{sc}$  with increasing 3C-SiC thickness suggests that thicker buffer layers may impede the movement of charge carriers, leading to reduced current generation inside the cell. Furthermore, a flattening is observed in both the  $V_{oc}$  and FF.  $V_{oc}$  represents the maximum voltage obtainable from the solar cell when no current is flowing, while FF indicates the efficiency of the cell in converting this voltage into useful energy. The flattening of  $V_{oc}$  and FF suggests that increasing the 3C-SiC thickness does not significantly impact these parameters within the studied range.

### 3.5 Effect of temperature

The operating temperature of solar cells is one of the primary factors influencing their performance. Understanding how solar cells respond to varying temperature conditions is crucial, especially given their frequent exposure to

a broad range of temperatures in terrestrial applications, typically ranging from 288 K to 323 K, and sometimes even higher. Fig. 7 illustrates the changes in  $J$ - $V$  characteristics of the device in relation to temperature variations. A notable observation is the decline in  $V_{oc}$ . As temperature rises, the internal carrier concentration within the semiconductor material also increases. This heightened carrier concentration results in an accelerated rate of electron-hole pair generation, leading to a higher saturation current. Since  $V_{oc}$  and the natural logarithm of the saturation current are negatively correlated, an increase in the saturation current at elevated temperatures consequently leads to a decrease in  $V_{oc}$  [42].

Fig. 8 highlights several key trends observed with increasing temperature in solar cell performance. Firstly, it shows a plateau in the  $J_{sc}$  and FF. This plateau suggests that there is a limit to the improvement of these parameters as temperature increases. While  $J_{sc}$  and FF may initially increase with rising temperature due to factors such as enhanced carrier generation and reduced series resistance,

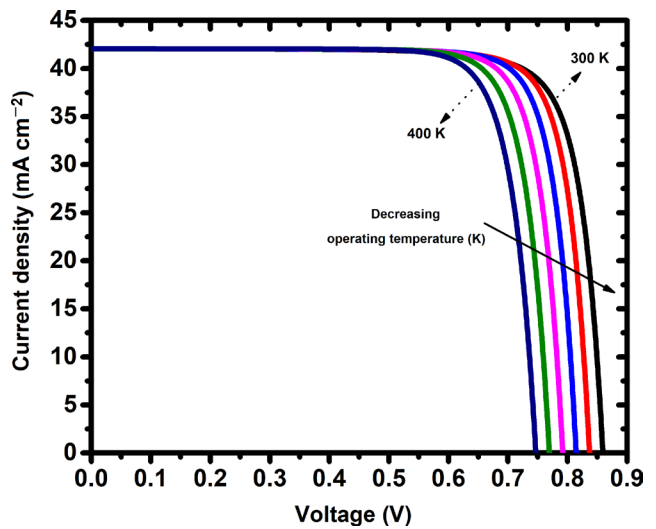


Fig. 7 Influence of temperatures on the  $J$ - $V$  characteristic

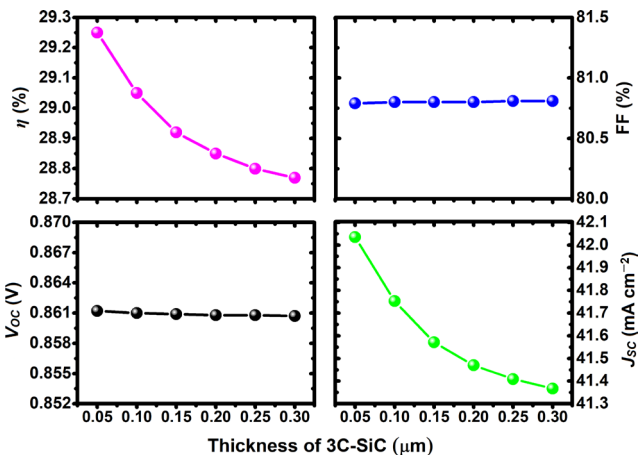


Fig. 6 Influence of 3C-SiC thickness on  $V_{oc}$ ,  $J_{sc}$ , FF, and  $\eta$

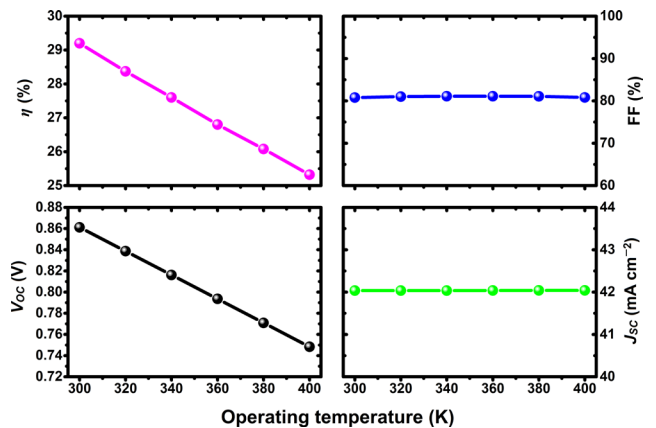


Fig. 8 Influence of temperatures on  $V_{oc}$ ,  $J_{sc}$ , FF, and  $\eta$

there comes a point where further increases in temperature do not result in significant improvements. This plateau effect underscores the complex interplay of various factors influencing solar cell performance, including carrier mobility and recombination rates. Additionally, Fig. 8 illustrates a decrease in  $\eta$  and  $V_{OC}$  with increasing temperature. This decline in  $\eta$  and  $V_{OC}$  is consistent with the observed decrease in performance at elevated temperatures. The decrease in  $V_{OC}$  can be linked to the rise in saturation current and higher intrinsic carrier concentration in the semiconductor material, as discussed previously. Similarly, the reduction in  $\eta$  reflects the combined effects of decreased  $V_{OC}$  and the plateau in  $J_{SC}$  and FF. A similar behavior of performance parameters was reported in [43].

Table 2 [2, 21, 22, 39, 41, 42, 44–47] and Fig. 9 show the outcomes of our simulation. The latter illustrates that our efforts have achieved an efficiency of 32.83%, representing a significant improvement of 40.18% compared to the reference efficiency of 23.42% obtained by incorporating  $\mu\text{c-Si:H}$  (BSF) into a conventional CIGS cell [21]. It is evident that cells with (PEDOT:PSS) BSF exhibit better performance compared to the basic cell with 3C-SiC as a buffer material. Table 2 presents the main results alongside those of other reported CIGS solar cells. Indeed, we have developed a novel configuration for a CIGS solar cell. The obtained results hold promise for researchers aiming to enhance device performance.

#### 4 Conclusion

In summary, this study presents a comprehensive computational investigation of a CIGS-based solar cell that

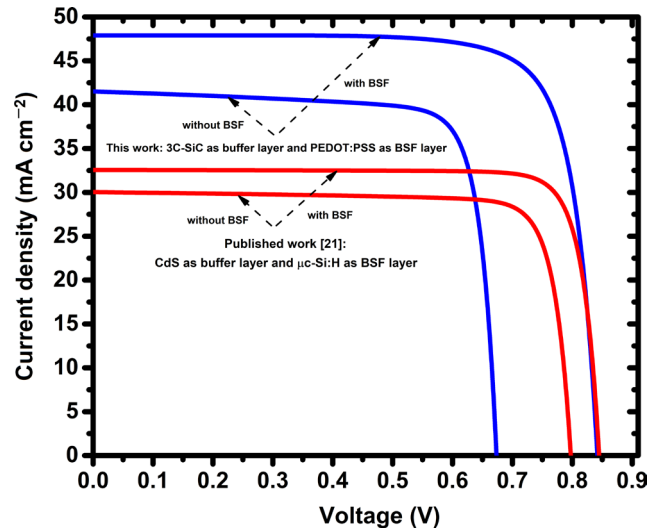


Fig. 9 BSF effect on the  $J$ - $V$  characteristics comparing by [21]

incorporates a 3C-SiC buffer layer and a PEDOT BSF layer, modelled using SCAPS-1D software [27]. The simulation results indicate that the ZnO/3C-SiC/CIGS/PEDOT/Mo heterostructure achieves a high photoconversion efficiency, with an optimal  $V_{OC}$  of 0.86 V,  $J_{SC}$  of  $56.40 \text{ mA cm}^{-2}$ , FF of 80.79%, and  $\eta$  of 32.83%. These values are consistent with and competitive against those reported in recent literature. Furthermore, we investigated the effects of key parameters, including the thicknesses of the CIGS absorber, the PEDOT BSF layer, and the 3C-SiC buffer, as well as the impact of temperature on device performance. Our findings emphasize the crucial role these factors play in optimizing cell efficiency. This study not only provides valuable insights into the optimization of CIGS-based solar cells but also highlights the potential of innovative material

Table 2 This work compared with other reported solar cells

No.	Type of research	Buffer/absorber layers	BSF layer	$\eta$ (%)	Ref.
1	Experimental	Si/Si	ZnS	6.40	[39]
2	Experimental	CdS/CIGS	MoSe <sub>2</sub>	9.00	[45]
3	Theoretical	CdS/CdTe	SnS	17.40	[41]
4	Theoretical	CdS/CIGS	Si	16.39	[42]
5	Theoretical	CdS/CIGS	$\mu\text{c-Si:H}$	23.42	[21]
6	Theoretical	CdS/CIGS	SnS	25.29	[44]
7	Theoretical	CdS/CIGS	CNGS*	29.39	[2]
8	Theoretical	3C-SiC/CIGS	–	25.51	[22]
9	Theoretical	3C-SiC/CdTe	–	17.29	[46]
Hybrid solar cell					
	Theoretical	PEDOT:PSS/GaAs	–	27.84	[47]
10	Theoretical	3C-SiC/CIGS	PEDOT: PSS	32.83	Our work

\* Copper nickel gallium selenide

combinations, such as 3C-SiC and PEDOT, to advance solar cell performance. Future research can build upon these findings by experimentally validating the proposed structure and investigating additional BSF and buffer materials to further enhance efficiency.

## References

- [1] Chargui, T., Lmai, F., AL-Hattab, M., Bajjou, O., Rahmani, K. "Experimental and numerical study of the CIGS/CdS heterojunction solar cell", *Optical Materials*, 140, 113849, 2023. <https://doi.org/10.1016/j.optmat.2023.113849>
- [2] Oublal, E., Al-Hattab, M., Ait Abdelkadir, A., Sahal, M., Kumar, N. "Photovoltaic efficacy of CNGS as BSF and second absorber for CIGS thin film solar cells- numerical approach by SCAPS-1D framework", *Materials Science and Engineering: B*, 305, 117401, 2024. <https://doi.org/10.1016/j.mseb.2024.117401>
- [3] Yoshikawa, K., Kawasaki, H., Yoshida, W., Irie, T., Konishi, K., Nakano, K., Uto, T., Adachi, D., Kanematsu, M., Uzu, H., Yamamoto, K. "Silicon heterojunction solar cell with interdigitated back contacts for a photoconversion efficiency over 26%", *Nature Energy*, 2(5), 17032, 2017. <https://doi.org/10.1038/nenergy.2017.32>
- [4] Green, M. A., Dunlop, E. D., Hohl-Ebinger, J., Yoshita, M., Kopidakis, N., Hao, X. "Solar cell efficiency tables (version 56)", *Progress in Photovoltaics: Research and Applications*, 28(7), pp. 629–638, 2020. <https://doi.org/10.1002/pip.3303>
- [5] Dris, K., Benhaliliba, M. "Novel Inorganic–Organic Heterojunction Solar Cell-Based Perovskite Using Two Absorbent Materials", *Nano*, 18(11), 2350091, 2023. <https://doi.org/10.1142/S1793292023500911>
- [6] Elbar, M., Tobbeche, S., Chala, S., Saidani, O., Kateb, M. N., Serdouk, M. R. "Effect of Temperature on the Performance of CGS/CIGS Tandem Solar Cell", *Journal of Nano- and Electronic Physics*, 15(1), 01020, 2023. [https://doi.org/10.21272/jnep.15\(1\).01020](https://doi.org/10.21272/jnep.15(1).01020)
- [7] Yousfi, A., Saidani, O., Messai, Z., Zouache, R., Meddah, M., Belgoumri, Y. "Design and Simulation of a Triple Absorber Layer Perovskite Solar Cell for High Conversion Efficiency", *East European Journal of Physics*, 4, pp. 137–146, 2023. <https://doi.org/10.26565/2312-4334-2023-4-14>
- [8] Dris, K., Benhaliliba, M. "Study and Optimization of a New Perovskite Solar Cell Structure Based on the Two Absorber Materials  $\text{Cs}_2\text{TiBr}_6$  and  $\text{MASnBr}_3$  Using SCAPS 1D", *Periodica Polytechnica Chemical Engineering*, 68(3), pp. 348–363, 2024. <https://doi.org/10.3311/PPch.36825>
- [9] Dris, K., Benhaliliba, M., Ayeshamariam, A., Roy, A., Kaviyarasu, K. "Improving the perovskite solar cell by insertion of methyl ammonium tin oxide and cesium tin chloride as absorber layers: scaps 1d study based on experimental studies", *Journal of Optics*, 2024. <https://doi.org/10.1007/s12596-024-01996-7>
- [10] Chen, Y., Tan, X., Peng, S., Xin, C., Delahoy, A. E., Chin, K. K., Zhang, C. "The Influence of Conduction Band Offset on CdTe Solar Cells", *Journal of Electronic Materials*, 47(2), pp. 1201–1207, 2018. <https://doi.org/10.1007/s11664-017-5850-9>
- [11] Uddin, M. S., Al Mashud, M. A., Toki, G. F. I., Pandey, R., Zulfiqar, M., Saidani, O., Chandran, K., Ouladsmane, M., Hossain, M. K. "Lead-free Ge-based perovskite solar cell incorporating  $\text{TiO}_2$  and  $\text{Cu}_2\text{O}$  charge transport layers harnessing over 25% efficiency", *Journal of Optics*, 53(4), pp. 3726–3742, 2024. <https://doi.org/10.1007/s12596-023-01570-7>
- [12] Dharmadasa, I. M. "Fermi level pinning and effects on  $\text{CuInGaSe}_2$ -based thin-film solar cells", *Semiconductor Science and Technology*, 24(5), 055016, 2009. <https://doi.org/10.1088/0268-1242/24/5/055016>
- [13] Fischer, J., Larsen, J. K., Guillot, J., Aida, Y., Eisenbarth, T., Regesch, D., Depredurand, V., Fevre, N., Siebentritt, S., Dale, P. J. "Composition dependent characterization of copper indium diselenide thin film solar cells synthesized from electrodeposited binary selenide precursor stacks", *Solar Energy Materials and Solar Cells*, 126, pp. 88–95, 2014. <https://doi.org/10.1016/j.solmat.2014.03.045>
- [14] Friedlmeier, T. M., Jackson, P., Bauer, A., Hariskos, D., Kiowski, O., Wuerz, R., Powalla, M. "Improved Photocurrent in  $\text{Cu(In, Ga)Se}_2$  Solar Cells: From 20.8% to 21.7% Efficiency with CdS Buffer and 21.0% Cd-Free", *IEEE Journal of Photovoltaics*, 5(5), pp. 1487–1491, 2015. <https://doi.org/10.1109/JPHOTOV.2015.2458039>
- [15] Hamri, Y. Z., Bourezig, Y., Medles, M., Ameri, M., Toumi, K., Ameri, I., Al-Douri, Y., Voon, C. H. "Improved efficiency of  $\text{Cu(In,Ga)Se}_2$  thinfilm solar cells using a buffer layer alternative to CdS", *Solar Energy*, 178, pp. 150–156, 2019. <https://doi.org/10.1016/j.solener.2018.12.023>
- [16] Loumachi, L., Yousfi, A., Saidani, O., Alsubaie, A. S., Abed, O., Amiri, S., Sahoo, G. S., Islam, M. R. "Strengthen the Power Conversion Efficiency of Solar Cell Based  $\text{RbGeI}_3$ : Numerical Approach", *East European Journal of Physics*, 3, pp. 416–424, 2024. <https://doi.org/10.26565/2312-4334-2024-3-50>
- [17] Nakada, T. "Invited Paper: CIGS-based thin film solar cells and modules: Unique material properties", *Electronic Materials Letters*, 8(2), pp. 179–185, 2012. <https://doi.org/10.1007/s13391-012-2034-x>

## Acknowledgements

The authors extend their appreciation to Taif University, Saudi Arabia, for supporting this work through project number (TU-DSPP-2024-106). This research was funded by Taif University, Saudi Arabia, Project No. TU-DSPP-2024-106.

- [18] Zouache, R., Bouchama, I., Saidani, O., Ghebouli, M. A., Akhtar, M. S., Saeed, M. A., Boudour, S., Lamiri, L., Belgherbi, O., Messaoudi, M. "CGS/CIGS single and triple-junction thin film solar cell: Optimization of CGS/CIGS solar cell at current matching point", *Micro and Nanostructures*, 189, 207812, 2024.  
<https://doi.org/10.1016/j.micrna.2024.207812>
- [19] Kanouni, L., Saidi, L., Yousfi, A., Saidani, O. "Performance Enhancement via Numerical Modeling and Optimization of FASnI3 Perovskite Solar Cell", *East European Journal of Physics*, 3, pp. 404–415, 2024.  
<https://doi.org/10.26565/2312-4334-2024-3-49>
- [20] Saidani, O., Yousfi, A., Samajdar, D. P., Xu, X., Biniyam Zemene, T., Bhattarai, S., Hossain, M. K., Sahoo, G. S. "Revealing the secrets of high performance lead-free CsSnCl<sub>3</sub> based perovskite solar cell: A dive into DFT and SCAPS-1D numerical insights", *Solar Energy Materials and Solar Cells*, 277, 113122, 2024.  
<https://doi.org/10.1016/j.solmat.2024.113122>
- [21] Zouache, R., Bouchama, I., Saidani, O., Djedoui, L., Zaidi, E. "Numerical study of high-efficiency CIGS solar cells by inserting a BSF  $\mu$ c-Si:H layer", *Journal of Computational Electronics*, 21(6), pp. 1386–1395, 2022.  
<https://doi.org/10.1007/s10825-022-01942-5>
- [22] Sobayel, M. K., Chowdhury, M. S., Hossain, T., Alkhamash, H. I., Islam, S., Shahiduzzaman, M., Akhtaruzzaman, M., Techato, K., Rashid, M. J. "Efficiency enhancement of CIGS solar cell by cubic silicon carbide as prospective buffer layer", *Solar Energy*, 224, pp. 271–278, 2021.  
<https://doi.org/10.1016/j.solener.2021.05.093>
- [23] Syväjärvi, M., Ma, Q., Jokubavicius, V., Galeckas, A., Sun, J., Liu, X., Jansson, M., ..., Svensson, B. G. "Cubic silicon carbide as a potential photovoltaic material", *Solar Energy Materials and Solar Cells*, 145, pp. 104–108, 2016.  
<https://doi.org/10.1016/j.solmat.2015.08.029>
- [24] Tarbi, A., Chtouki, T., Sellam, M. A., Benahmed, A., El Kouari, Y., Erguig, H., Migalska-Zalas, A., Goncharova, I., Taboukhat, S. "Optimization of ultra-thin CIGS-based solar cells by strained In<sub>1-x</sub>Ga<sub>x</sub>As absorption layer: 1D SCAPS modeling", *Journal of Computational Electronics*, 22(4), pp. 1089–1096, 2023.  
<https://doi.org/10.1007/s10825-023-02040-w>
- [25] Monika, Pradhan, P., Amrute, V., Chanda, A. "Structural and optical study of conducting polymer PEDOT:PSS and its composite with GO", *Materials Today: Proceedings*, 2023.  
<https://doi.org/10.1016/j.matpr.2023.07.123>
- [26] Hu, L., Song, J., Yin, X., Su, Z., Li, Z. "Research Progress on Polymer Solar Cells Based on PEDOT:PSS Electrodes", *Polymers*, 12(1), 145, 2020.  
<https://doi.org/10.3390/polym12010145>
- [27] Niemegeers, A., Burgelman, M., Decock, K., Degrave, S., Verschraegen, J. "SCAPS-1D: Solar Cell Capacitance Simulator, (3.3.10)", [computer program] Available at: [scaps.elis.ugent.be](https://scaps.elis.ugent.be) [Accessed: 06 November 2025]
- [28] Saidani, O., Abderrahim, Y., Zitouni, M., Sahoo, G. S., Zouache, R., Mohammad, M. R., Alothman, A. A., Mohammad, S., Vimalan, M., Toki, G. F. I., Hossain, M. K. "Numerical study of high-performance lead-free CsSnCl<sub>3</sub>-based perovskite solar cells", *Journal of Optics*, 2024.  
<https://doi.org/10.1007/s12596-024-01817-x>
- [29] Islam, M. S., Rashid, M. J., Akhtaruzzaman, M., Takashi, S., Kazmi, J., Karim, M. R., Alnaser, I. A., Sobayel, K. "Exploration of Cd<sub>1-x</sub>Zn<sub>x</sub>Se as a window layer for CIGS based solar cell with PEDOT: PSS as back surface field layer", *Materials Research Express*, 10(12), 126405, 2024.  
<https://doi.org/10.1088/2053-1591/ad17ee>
- [30] Patel, A. K., Mishra, R., Soni, S. K. "Electrical and optical parameters optimization and interface engineering for efficiency improvement of double CIGS absorber based solar cell", *Solar Energy*, 257, pp. 125–136, 2023.  
<https://doi.org/10.1016/j.solener.2023.04.034>
- [31] Gohri, S., Madan, J., Pandey, R. "Augmenting CIGS Solar Cell Efficiency Through Multiple Grading Profile Analysis", *Journal of Electronic Materials*, 52(9), pp. 6335–6349, 2023.  
<https://doi.org/10.1007/s11664-023-10567-8>
- [32] Ghalmi, L., Bensmaïne, S., Merzouk, C. E. H. "Numerical Simulation Study of CIGS-based Thin Film and Heterojunction Solar Cells: Doping and Buffer/Absorber Layer Optimization for Maximum Efficiency", *Journal of Renewable Energies*, 1(1), pp. 51–63, 2023.  
<https://doi.org/10.54966/jreen.v1i1.1098>
- [33] Moustafa, M., Yasin, S., Swillam, M. "Boosting Efficiency Up to 34.5% of CIGS-Based Solar Cells Using a New Heterostructure by Simulation", *Romanian Journal of Physics*, 68, 621, 2023.  
<https://doi.org/10.59277/romjphys.2023.68.621>
- [34] N'guessan, A. I., Bouich, A., Touré, A., Soucasse, B. M., Soro, D. "Influence of Sulfur Content in Zn(O,S) Buffer Layer onto Copper Indium Gallium Sulfur-Based Solar Cells Through Surface Engineering at ZnO<sub>1-x</sub>S<sub>x</sub>/CIGS Interface", *JOM*, 75(10), pp. 4332–4340, 2023.  
<https://doi.org/10.1007/s11837-023-06018-8>
- [35] Yousfi, A., Bencherif, H., Dehimi, L., Pezzimenti, F., Saidi, L., Abdi, M. A., Meddour, F., Khezzer, D. "Possible efficiency boosting of tandem solar cell by using single antireflection coating and BSF layer", In: 2019 1st International Conference on Sustainable Renewable Energy Systems and Applications (ICSRESA), Tebessa, Algeria, 2019, pp. 1–4. ISBN 978-1-7281-5357-5  
<https://doi.org/10.1109/ICSRESA49121.2019.9182619>
- [36] Rawat, S., Gohri, S., Madan, J., Pandey, R. "Insight on PV parameters on CIGS solar cell under different grading profiles", *Materials Today: Proceedings*, 2023.  
<https://doi.org/10.1016/j.matpr.2023.04.229>
- [37] Deo, M., Chauhan, R. K. "Tweaking the performance of thin film CIGS solar cell using InP as buffer layer", *Optik*, 273, 170357, 2023.  
<https://doi.org/10.1016/j.ijleo.2022.170357>
- [38] Yadav, T., Yadav, S., Sahu, A. "Comparative performance analysis of perovskite/CIGS-based double absorber layer solar cell with BaSi<sub>2</sub> as a BSF layer", *Journal of Optics*, 53(4), pp. 2922–2929, 2024.  
<https://doi.org/10.1007/s12596-023-01425-1>
- [39] Albiss, B., Al-Widyan, M. "Numerical Simulation, Preparation, and Evaluation of Cu(In,Ga)Se<sub>2</sub> (CIGS) Thin-Film Solar Cells", *ChemEngineering*, 7(5), 87, 2023.  
<https://doi.org/10.3390/chemengineering7050087>

- [40] Yang, X., Chen, B., Chen, J., Zhang, Y., Liu, W., Sun, Y. "ZnS thin film functionalized as back surface field in Si solar cells", *Materials Science in Semiconductor Processing*, 74, pp. 309–312, 2018.  
<https://doi.org/10.1016/j.mssp.2017.08.011>
- [41] Kohara, N., Nishiwaki, S., Hashimoto, Y., Negami, T., Wada, T. "Electrical properties of the Cu(In,Ga)Se<sub>2</sub>/MoSe<sub>2</sub>/Mo structure", *Solar Energy Materials and Solar Cells*, 67(1–4), pp. 209–215, 2001.  
[https://doi.org/10.1016/S0927-0248\(00\)00283-X](https://doi.org/10.1016/S0927-0248(00)00283-X)
- [42] Benabbas, S., Rouabah, Z., Bouarissa, N., Chelali, N. "The role of back surface field SnS layer in improvement of efficiency of CdTe thin film solar cells", *Optik*, 127(15), pp. 6210–6217, 2016.  
<https://doi.org/10.1016/j.ijleo.2016.04.050>
- [43] Fathi, M., Abderrezek, M., Djahli, F., Ayad, M. "Study of Thin Film Solar Cells in High Temperature Condition", *Energy Procedia*, 74, pp. 1410–1417, 2015.  
<https://doi.org/10.1016/j.egypro.2015.07.788>
- [44] Heriche, H., Rouabah, Z., Bouarissa, N. "New ultra-thin CIGS structure solar cells using SCAPS simulation program", *International Journal of Hydrogen Energy*, 42(15), pp. 9524–9532, 2017.  
<https://doi.org/10.1016/j.ijhydene.2017.02.099>
- [45] Naceri, L., Belarbi, M. "Theoretical analysis of introducing CeOx as a passivation layer: an innovative approach to boosting CIGS solar cell efficiency", *Physica Scripta*, 99(3), 035028, 2024.  
<https://doi.org/10.1088/1402-4896/ad2824>
- [46] Sameera, J. N., Islam, M. A., Islam, S., Hossain, T., Sobayel, M. K., Akhtaruzzaman, M., Amin, N., Rashid, M. J. "Cubic Silicon Carbide (3C–SiC) as a buffer layer for high efficiency and highly stable CdTe solar cell", *Optical Materials*, 123, 111911, 2022.  
<https://doi.org/10.1016/j.optmat.2021.111911>
- [47] Wu, P., Zhao, F., Cui, L., Pan, S., Su, N., Yang, H., Yu, Y., Chen, M., Yi, Z., Cai, S. "Realization of 27.84% efficiency of the GaAs/PEDOT: PSS thin-film hybrid solar cell based on high solar energy absorption", *Solar Energy*, 164, 109532, 2023.  
<https://doi.org/10.1016/j.optlastec.2023.109532>